JACS
JOURNAL OF THE AMERICAN CHEMICAL SOCIETY
pubs.acs.org/JACS
Article

# Supramolecular Polymers Controlled by Glycan Geometry

Xiaomei Liu, Liman Zhao, Pingping Niu, Ya Zeng, Yiwei Shi, Xinyu Bian, Yating Liu, Shengjie Ling, Long Li,* and Guosong Chen*

Cite This: J. Am. Chem. Soc. 2026, 148, 8331−8340

Read Online

ACCESS | Metrics & More | Article Recommendations | Supporting Information

**ABSTRACT:** Despite the crucial roles of glycan structures in glycosylated macromolecules such as proteoglycans in the extracellular matrix, their regulatory mechanism is still poorly understood, due to the complex structures and dynamic interactions of polysaccharides. Here, supramolecular polymers were employed as simplified mimics for fibrous proteoglycans to investigate the regulatory role of the glycans. We constructed a series of glycopeptides based on the precise linear tetrasaccharide structure (CT) from chondroitin. Experimental and computational results indicated that glycopeptides containing triphenylalanine and chondroitin tetrasaccharide (CT-3F) could assemble into tetra-stranded nonhelical fibers. Compared with the glycopeptide fiber of nonlinear sialyllactose (SL-3F), the linear geometry of CT resulted in fewer hydrogen bonds than nonlinear SL, and consequently different flexibility of the corresponding supramolecular glycopolymers which was supported by the change of measured persistence length and bending modulus. Importantly, flexibility of CT-3F fibers from glycan geometry could significantly enhance their interaction with preosteoblastic cells and osteogenic gene expression. These results reveal an unexplored dimension of complex oligosaccharides and provide an alternative pathway for tuning the properties of supramolecular polymers and even related biomaterials.

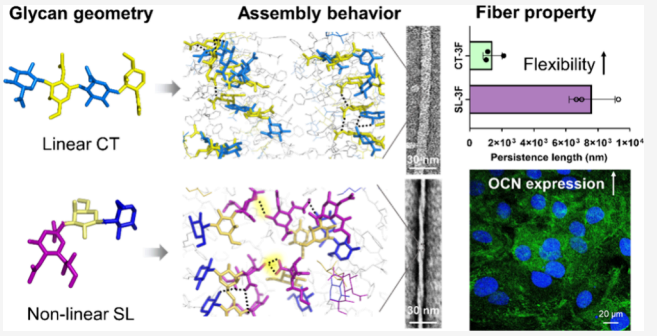




## INTRODUCTION

Glycosylation is one of the most prevalent and diverse post-translational modification in protein biosynthesis, in which glycans are transferred to proteins by glycosyltransferases.[1] Because of their diverse monomers and linkage modes, glycans exhibit much higher complexity than proteins. The glycosylation process enriches protein repertoire beyond that dictated by the amino acid sequence, and it can alter the structural features of proteins.[2,3] Proteoglycans (PGs), consisted of a protein core with quite a few of covalently modified polysaccharide chains, widely exist in the extracellular matrix (ECM), the plasma membrane and secretory granules.[4] As important components for the pericellular space, PGs are actively involved in cell adhesion, signaling, and other biological processes, which can be modulated both by their chemical composite and physical properties.[5] For instance, glycans on PGs were proven to interact with SARS-CoV-2 spike protein and participate into the infection process of COVID-19.[6] These glycosylated macromolecules are also considered as the key regulator of mechanics and viscoelasticity of ECM based on their fibrous structures.[7] Although increasing attention has been drawn to the glycan roles in modulating physical and biological properties of PGs, elucidating the precise regulatory mechanisms at the molecular level remains challenging due to their heterogeneity, high molecular weight, diverse monosaccharide constituents and varied modification patterns.[8,9]

To precisely understand such fibrous structures based on proteoglycans, supramolecular glycopolymers can be employed as a kind of mimicking model.[10−12] On one hand, the precise molecular structure of monomers, for example, glycopeptide, can build fibrous structures and even materials from molecular understanding.[13−17] Meanwhile, by virtue of their well-defined structures, these supramolecular fibrous glycoassemblies provide regulation handle for further understanding on their physical properties for biological functions.[18−20] However, investigation into the glycan structures of supramolecular glycopolymers is little due to the complicated preparation procedures of oligosaccharides. While the oligopeptide components have been extensively studied, the structural diversity of oligosaccharides has been largely overlooked. To the best of our knowledge, no studies on the contribution from oligosaccharide structure to the physical property and even

Received: October 22, 2025
Revised: February 3, 2026
Accepted: February 6, 2026
Published: February 19, 2026

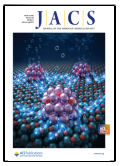




https://doi.org/10.1021/jacs.5c18638
J. Am. Chem. Soc. 2026, 148, 8331−8340

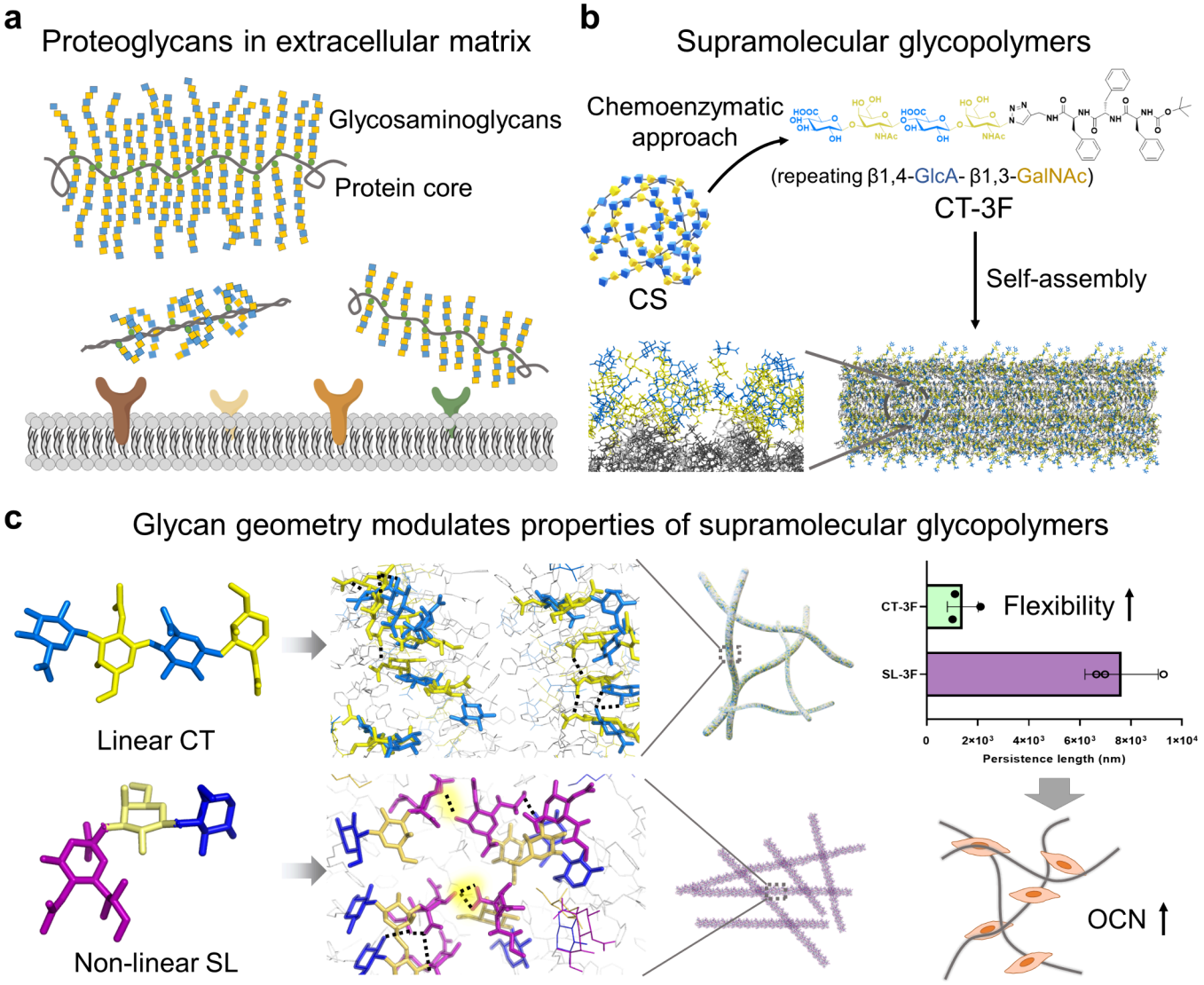


**Figure 1.** (a) Structure presentation of PGs in the ECM. PGs consist of a core protein (shown in brown) with covalently attached glycosaminoglycan chains. Glycosaminoglycans vary in length and conformation, thereby influencing the properties of PGs and their interactions with receptors (shown in different color) on the cell membrane (shown in gray). (b) Design and construction of supramolecular glycopolymers based on CT-peptides to mimic PGs. CT-3F was synthesized via chemoenzymatic approach. Composed of triphenylalanine and chondroitin tetrasaccharide, this glycopeptide self-assembles into fibers in water, featuring oligopeptide cores covalently decorated with oligosaccharides and serving as simplified mimics of PGs in ECM. (c) Scheme for this work. In this work, to explore the influence of glycan geometry, supramolecular polymers with linear CT and nonlinear SL were compared from the molecular level to macroscopic mechanical and biological properties.

biofunctions of supramolecular polymers can be found in the literature.

Here, we designed and constructed a series of glycopeptides (CT-peptides) based on linear chondroitin tetrasaccharide (CT) through a chemoenzymatic approach (Figure 1a and 1b). CT was derived from chondroitin polysaccharides (CS), the widespread glycosaminoglycans attached to protein cores of PGs and closely related with bone homeostasis.[21] By combining experimental results and all-atom molecular dynamics simulation, glycopeptides containing triphenylalanine and chondroitin tetrasaccharide (CT-3F) were found to form tetra-stranded nonhelical fibers. Focusing on the influence of glycan structures, CT-3F fibers with linear oligosaccharide were compared with SL-3F fibers containing nonlinear sialyllactopyranoside (SL) and the same oligopeptide (Figure 1c). The results showed that glycan geometry had significant influence on their assembly behaviors. The linear geometry of CT led to less hydrogen bonds and enhanced flexibility of fibrous structures characterized by shorter persistence length, compared with the nonlinear SL. Furthermore, through incubating with mouse preosteoblastic MC3T3-E1 cells, increased flexibility of CT-3F fibers from glycan geometry was found to enhance interaction with cells and osteogenic gene expression. In short, this work demonstrated that glycan geometry could serve as primary determinant of supramolecular polymers and represented an alternative approach for modulating their properties and even related functions as biomaterials. To date, glycans are primarily considered as hydrophilic moieties in the design of supramolecular materials, while the influence of glycan structure itself on supramolecular assembly such as fibers has been rarely addressed. Glycans possess pronounced stereochemical and regiochemical diversity, which gives rise to their structural complexity and renders molecular-level investigations of the


https://doi.org/10.1021/jacs.5c18638
J. Am. Chem. Soc. 2026, 148, 8331−8340

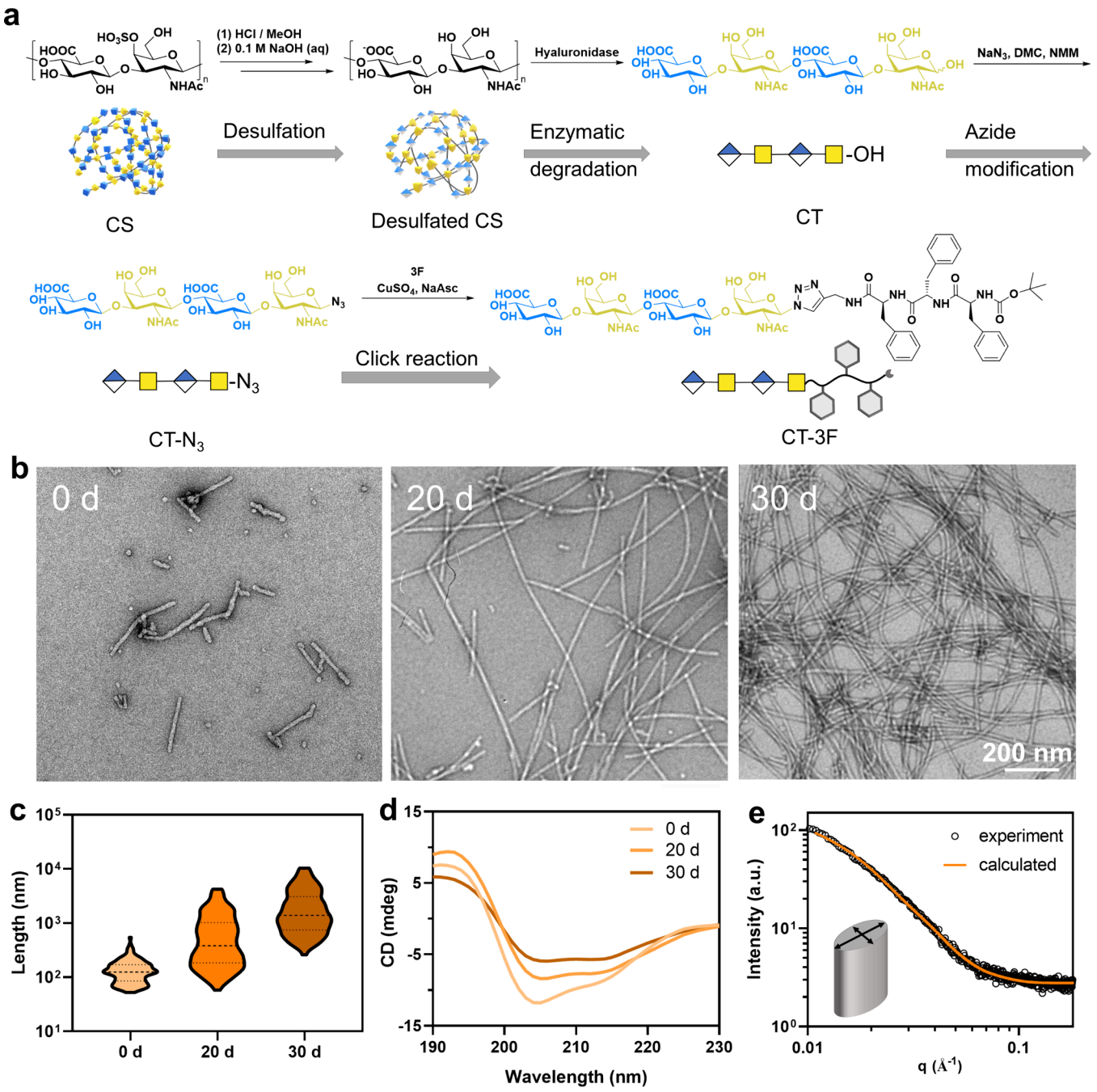


**Figure 2.** (a) Synthetic procedure of CT-3F. [Legend: DMC, 2-chloro-1,3-dimethylimidazolidinium chloride; NMM, 4-methylmorpholine; NaAsc, sodium L-ascorbate.] The structure of 3F was described in the Supporting Information. (b) TEM images, (c) statistical results for fiber length, and (d) CD spectra at different assembly time for CT-3F assemblies. (e) SAXS result and its calculated result for CT-3F assemblies at 30 d. The SAXS pattern was fitted to an elliptical cylinder model.

regulatory role of glycans particularly challenging. In light of this complexity, the present work adopted a simplified strategy: starting from molecular structures, we moved beyond atomic-level details to examine how the spatial arrangement of glycans influences their assembly behavior from a higher-level structural perspective.

## RESULTS AND DISCUSSION

### Supramolecular Glycopolymers Based on CT-3F

We chose triphenylalanine (3F), a widely utilized assembly building block,[22−24] as the oligopeptide part and designed CT-3F glycopeptide to construct supramolecular glycopolymers in water to mimic PGs in ECM (Figure 2a). The precise tetrasaccharide (CT), based on repeating $\beta$-1, 4-linked D-glucuronic acid and $\beta$-1, 3-linked *N*-acetyl D-galactosamine disaccharide units ($\beta$1, 4-GlcA-$\beta$1, 3-GalNAc) of natural CS, was obtained through enzymatic degradation of desulfated polysaccharides by hyaluronidase. Then, these tetrasaccharides were chemically functionalized with azide groups on the reducing end, followed by a click reaction with oligopeptides. The detailed synthetic procedures are provided in the Supporting Information. The assembly process of CT-3F was traced through TEM (Figure 2b). After dispersed in water,



https://doi.org/10.1021/jacs.5c18638
J. Am. Chem. Soc. 2026, 148, 8331−8340

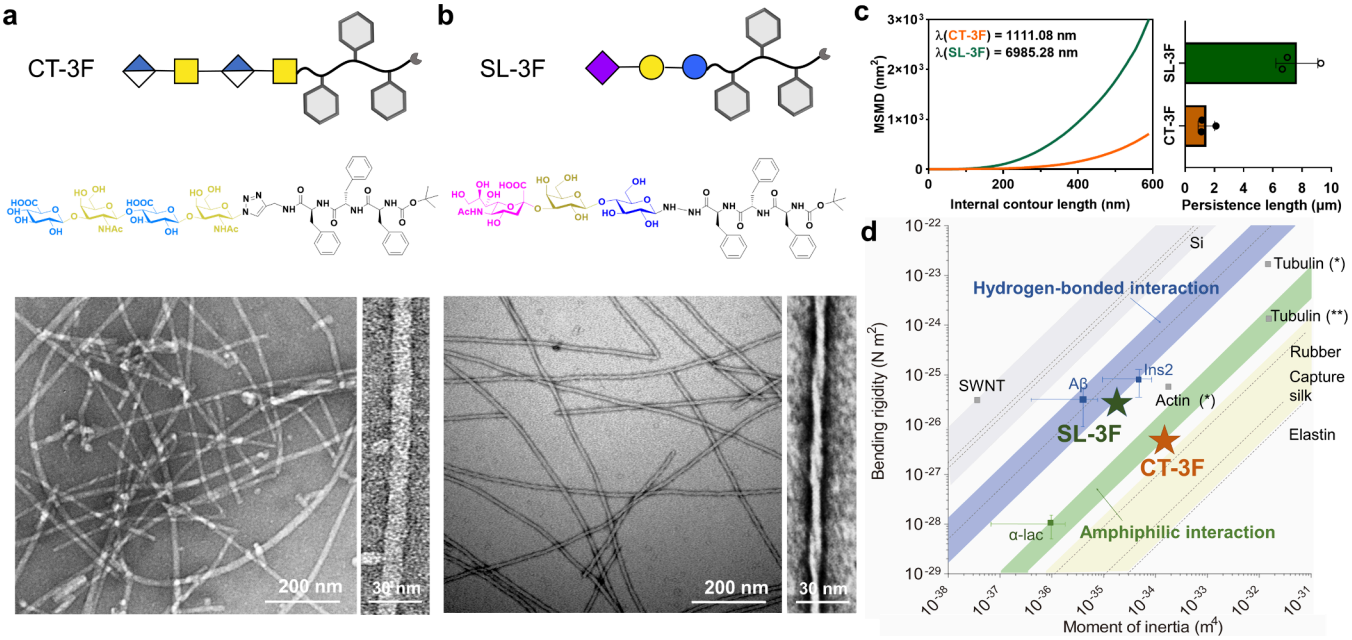


**Figure 3.** Comparison between CT-3F and SL-3F fibers. The simplified cartoon structural model (above), chemical structure (middle) and TEM images (below) for (a) CT-3F and (b) SL-3F. (c) Plot of mean-squared midpoint displacement (MSMD) versus internal contour length[28] with resulting persistence lengths (left) and its corresponding statistic results (right) for CT-3F and SL-3F fibers. (d) Comparison plots of bending rigidity versus moment of inertia for different classes of fibers. The gray bands represent covalent and metallic materials. The blue band was for hydrogen-bonded fibrous nanostructures. The green band was for materials held together by amphiphilic interactions, and the yellow band was for fibers with predominantly entropic elasticity. [Except CT-3F and SL-3F, the other part of panel (d) was adapted with permission from ref 30. Copyright 2007, The American Association for the Advancement of Science.]

CT-3F assembled into short rods with a length of about 200 nm at first. After further incubation under room temperature, these short rods gradually transformed into nonhelical long fibers with contour length up to micrometers, which was supported by the statistical results of fiber length (see Figure 2c, as well as Figure S8). DLS results also revealed that the size of CT-3F assembly had a significant shift to the microscale over time (Figure S9). Circular dichroism (CD) spectra were used to investigate the molecular packing in the glycoassemblies at different assembly times (Figure 2d). CD spectra all showed two separated negative peaks around 210 nm, which indicated that both short rods and long fibers adopted a similar $\alpha$-helix conformation at the molecular level, although their supramolecular morphologies are nonhelical (Figure S10). Furthermore, methanol was employed to accelerate the formation of fibers[25] with different ratio, and then volatilized under room temperature. The addition and volatilization of 10% methanol resulted in the formation of long fibers within 3 days, which largely accelerated the assembly process of CT-3F (Figure S11). The morphology of these glycoassemblies was thoroughly investigated by the combination of TEM, AFM, small-angle X-ray scattering (SAXS), and cryotransmission electron microscopy (cryo-TEM). The observation of TEM exhibited that short rods and nonhelical long fibers had the same width of around 11 nm (Figure S12). The results of AFM showed that both short rods and long fibers were in the height range of about 3.6 nm (Figure S13). SAXS was also employed to characterize the fiber morphology, and the fitting result showed good agreement with the elliptical cylinder model (see Figure 2e, as well as Figure S14). These results indicated that these two glycoassemblies had the same elliptical cross-section with the major axis measuring about 11 nm and the minor axis measuring about 4 nm, which was further observed through cryo-TEM (Figure S15).

## Glycan Geometry Influenced Mechanical Properties of Fibrous Structures

In previous work,[26] we investigated assembly behavior and underlying molecular mechanism of glycopeptide SL-3F, composed of sialyllactose (SL) and triphenylalanine (Figure 3b). Although sharing the same oligopeptide sequence, SL-3F assembled into double-stranded helical fibers exhibiting a smaller cross-sectional dimension compared to the nonhelical fibers formed by CT-3F (see Figure 3a and 3b, as well as Figure S16a). The contour length of SL-3F fibers was up to micrometers (Figure S16b). SAXS profiles also indicated a reduced degree of cross-sectional anisotropy in SL-3F fibers (Figure S17). We further analyzed fiber flexibility by examining persistence length ($\lambda$), the length above which thermal fluctuations can buckle fibrous structures.[27,28] Quantitative analysis of mean-square midpoint displacement (Figure 3c) revealed that the persistence length of CT-3F fibers (approximately 1.1 $\mu$m) was significantly shorter than that of twisted SL-3F fibers (approximately 7.0 $\mu$m). Correspondingly, analysis of the mean square end-to-end distance (MSED) showed distinct differences between the two assemblies, with MSED of about 1.3 $\mu$m for CT-3F and 6.5 $\mu$m for SL-3F fibers (Figure S18). Moreover, the bending modulus ($\kappa$) of the fibers was calculated using the relationship $\kappa = k_B T\lambda$, where $k_B$ denotes Boltzmann's constant and $T$ represents temperature.[29] Additionally, the cross-sectional moments of inertia ($I$) were calculated according to its definition $I = \iint_A r^2\, dA$, where $r$ is the distance between the center of the section and $A$ is the calculated area. Detailed calculation process was presented in Section 4.2 in the Supporting Information. The cross-sectional moments of inertia $I$ were further plotted against $\kappa$ alongside



https://doi.org/10.1021/jacs.5c18638
J. Am. Chem. Soc. 2026, 148, 8331−8340

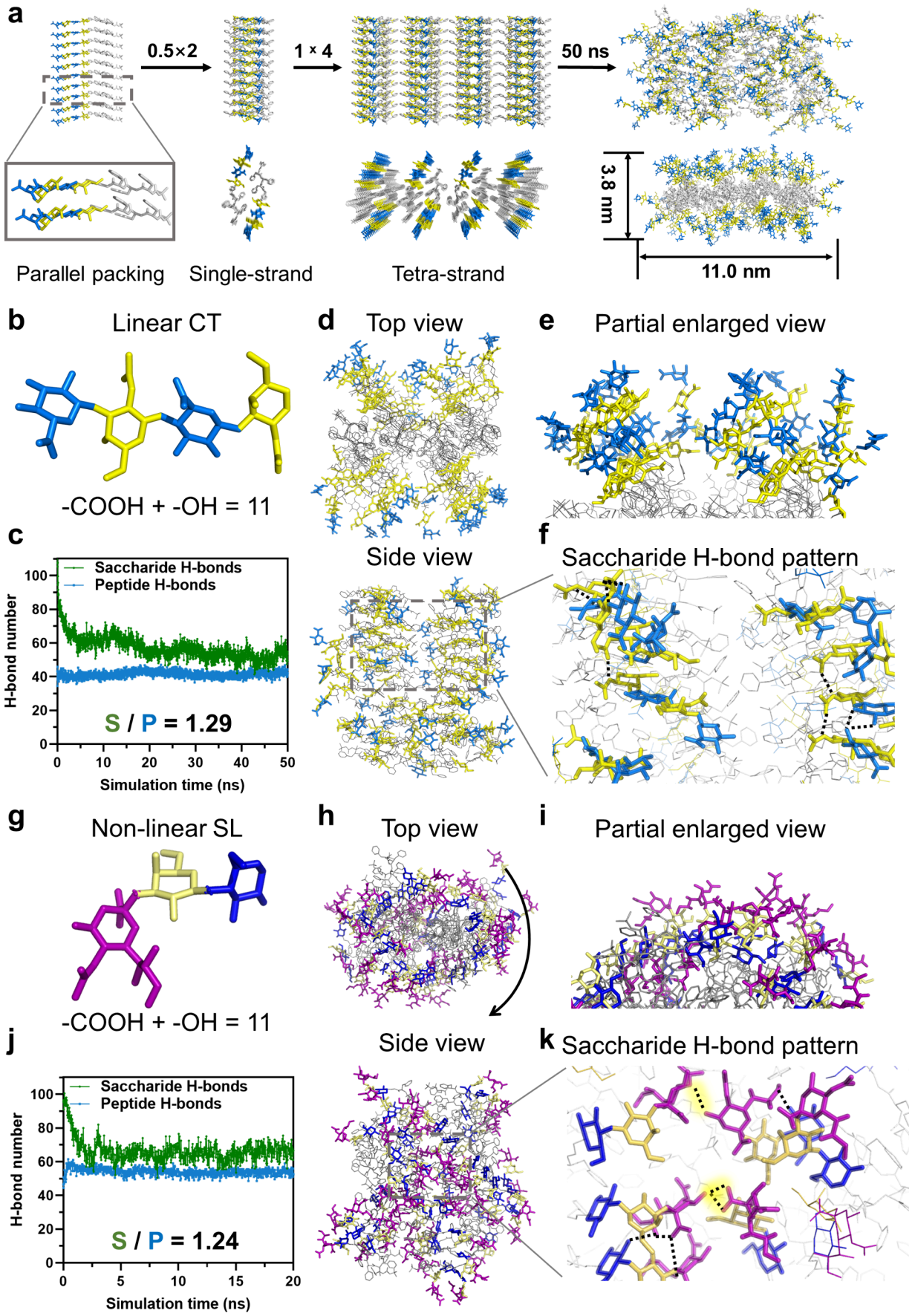


**Figure 4.** Influence of glycan geometry on the assembly of glycopeptide fibers. (a) The construction process of CT-3F fibers. (b and g) Oligosaccharide geometry for CT (b) and SL (g). (c and j) The statistical results of two types of H-bonds for CT-3F (c) and SL-3F (j). (d and h)



https://doi.org/10.1021/jacs.5c18638
J. Am. Chem. Soc. 2026, 148, 8331−8340

**Figure** 4. continued

Simulation results for CT-3F (d) and SL-3F (h). (e and i) Partial views for CT-3F (e) and SL-3F (i). (f and k) Intermolecular saccharide H-bond patterns for CT-3F (f) and SL-3F (k). For better visualization, the oligopeptide part was colored with silver, and the oligosaccharide part from different strands was colored with different colors. H-bonds were marked with dashed lines, and saccharide H-bonds between different strands were highlighted. CT-3F fiber was partially shown as a double-strand state for comparison with SL-3F one.

other fibrous systems (Figure 3d). The elastic modulus ($Y$) could be estimated from this plotted figure based on the equation $Y = \kappa/I$.[30] It was shown that SL-3F fibers lay in the region for hydrogen-bonded nanostructures, while CT-3F fibers were closer to materials held together by amphiphilic interactions, indicating that intramolecular interactions between CT-3F fibers were much weaker than those of SL-3F fibers. Collectively, these intrinsic mechanical measurements consistently demonstrated that CT-3F fibers were more compliant than SL-3F fibers, exhibiting a lower bending rigidity and higher flexibility.

To find out how different oligosaccharide parts led to these distinct fibrous structures, molecular dynamics (MD) simulation of these two glycopeptide fibers was conducted under the same protocol. To facilitate saccharide H-bonds (hydrogen bonds) formation, these glycopeptides were arranged in a parallel manner to obtain consequently higher stability than conventional antiparallel states for 3F.[26] To be more exact, glycopeptide amphiphiles adopted an identical orientation in axial stacking to construct half-strand protofibrils, which were further dimerized into single-strand protofibrils (Figure 4a). These single-strand protofibrils were then placed as tetra-strand fibrils to accord with the experimental measurements of CT-3F fibers above. After 50 ns simulation, a stable fibrous structure emerged with an elliptical cross-section of 11.0 ± 0.3 nm in the major axis and 3.8 ± 0.1 nm in the minor axis (Figure S19). Besides, the simulation results showed that CT-3F fibers had no twisting tendency with the linear geometry of CT (Figure 4b), which was consistent with the experimental observation. To further understand the driving force of the assembly process, the role of each phenylalanine residue in CT-3F was identified through the calculation of solvent accessible surface area (SASA). The result showed that the driving force for strand formation was larger than the one for strand association, indicating the formation of long fibers with a high aspect ratio (Figures S20−S22). Moreover, the double-strand model was constructed and compared with the tetrastrand structure of CT-3F fibers (Figure S23). Negligible change was found in SASA, while a significant increase of saccharide H-bonds was observed, suggesting its important role in glycopeptide assembly (Figure S24 and S25). To further confirm the importance of H-bonds in the formation of fibers, we examined the assembly behavior of CT-3F under H-bond-suppressing conditions (Figure S26). The result showed that the presence of guanidinium hydrochloride significantly inhibited fiber growth, highlighting the essential contribution of H-bonds to the formation of fibrous structures.

For SL-3F fibers, glycopeptides were arranged into double-strand models in the same way with CT-3F due to their identical oligopeptide parts (Figures S27 and S28). However, unlike nonhelical CT-3F fibers, distinct helical behavior of SL-3F fibers was observed during MD simulation (Figure 4g). Based on these two successful fibrous models, we next explored how the oligosaccharide part influenced their mechanical properties from the molecular level. First, the SASA of phenylalanine residues in SL-3F fibers was analyzed and showed the similar distribution with the one in CT-3F fibers (Figure S29). The SASA of the middle phenylalanine residue was larger than those of the other ones. Furthermore, H-bond distributions in these two fibers were quantitatively analyzed and compared. The similar number ratio of saccharide H-bonds to peptide H-bonds (S/P value) was observed, which was 1.29 for CT-3F and 1.24 for SL-3F (Figure 4c and 4j). These results indicated a similar balance between oligosaccharides and oligopeptides in these two structures, consistent with the emergency of long fibers for both CT-3F and SL-3F.

However, such a dramatic difference between these two glycopeptide fibers can be attributed to glycan geometry, since it can be very different. The oligosaccharide parts in SL-3F fibers were found to exhibit nonlinear configuration, which was distinct from molecular geometry of linear CT (see Figure 4b and 4g). This difference in the glycan configuration was further verified through density functional theory (DFT) calculations of the corresponding oligosaccharides (Figure S30). Moreover, the most significant difference of the results from simulation between these two fibers came from the H-bonds, i.e., the number of H-bonds in CT-3F fibers was significantly less than that in SL-3F fibers (Figure 4c and 4j). The saccharide H-bond patterns between strands in these two fibers were also found to be quite different. When certain molecules with the same number of H-bond formation groups were further examined, it was clearly found that these two oligosaccharides contributed to distinct H-bonding networks with different molecular geometries (Figure 4f and 4k). In CT-3F fibers, linear saccharides were relatively dispersed surrounding the peptide backbone, whereas nonlinear saccharides in SL-3F fibers formed an interwoven hydrogen-bonding network. The expanded structure of linear CT conferred greater spatial flexibility than converging states of nonlinear SL, resulting in less H-bond formation (see Figure 4e and 4i). The analysis of the root-mean-square fluctuation (RMSF) was further employed to evaluate molecular dynamics by measuring the average displacement of oligosaccharides. The RMSF values for these two glycoassemblies showed that linear CT had higher degree of dynamics than nonlinear SL (Figure S31), indicating weaker interactions between CT than the ones between SL. Their difference in H-bond formation was further experimentally supported by the FT-IR spectra (Figure S32). Furthermore, we investigated the influence of breaking the H-bond on the stability of these two fibers via CD spectra and TEM observation (Figures S33 and S34). It was found that SL-3F fibers were more sensitive to H-bond disruption, which confirmed our simulation results. The thermal stability of the fibers was also investigated. Both CT-3F and SL-3F fibers dissociated upon heating to 80 °C, demonstrating a similar thermal stability threshold (see Figures S35 and S36).

Considering the carboxylic acid groups in CT, one may wonder the contribution from electrostatic repulsions, which may weaken the H-bond forming ability of CT. Therefore, a CT-3F double-strand protofibril model with no charge was constructed (Figure S37). The results showed that saccharide H-bonds had only a slight increase, indicating that charge



https://doi.org/10.1021/jacs.5c18638
J. Am. Chem. Soc. 2026, 148, 8331−8340

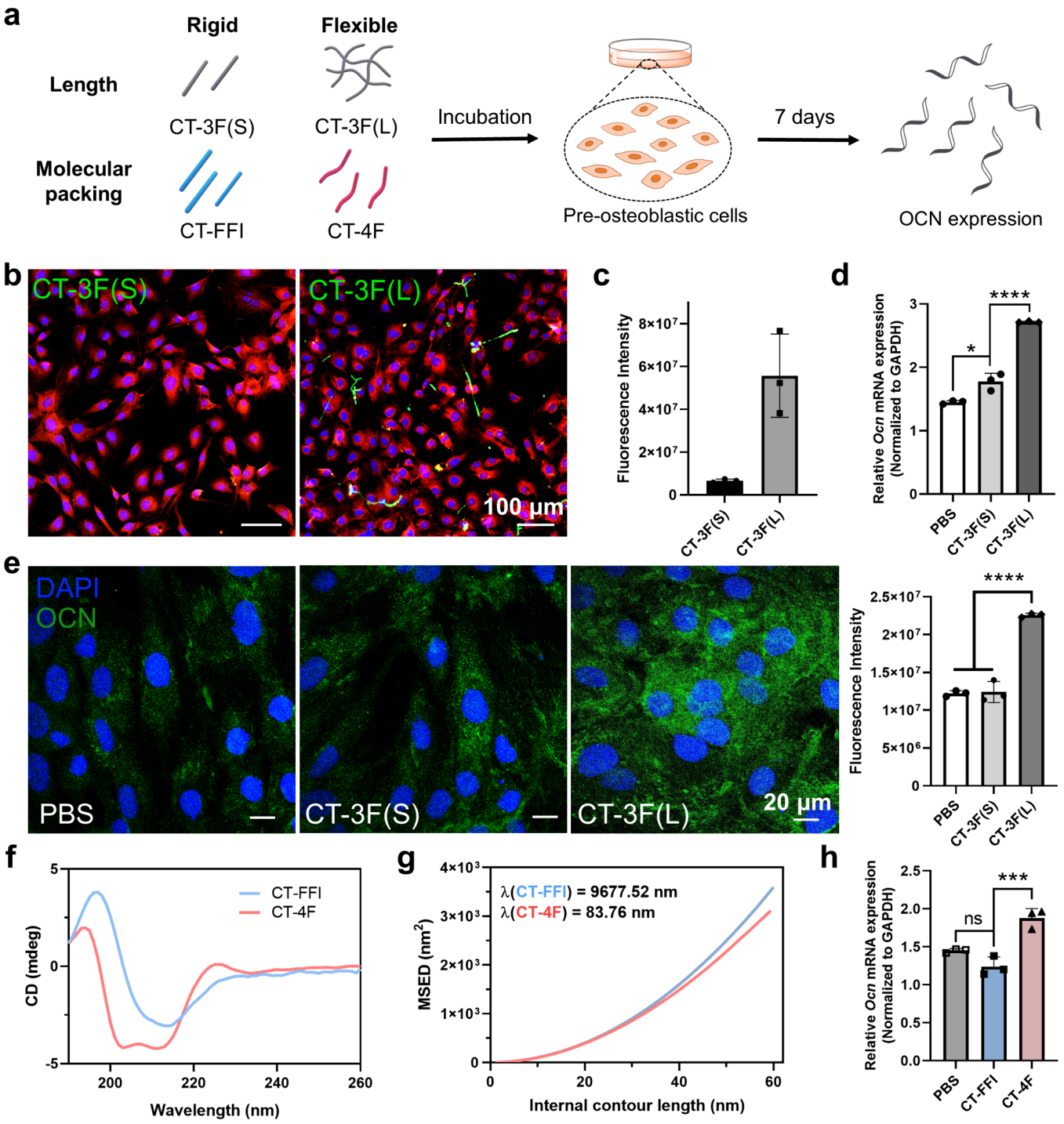


**Figure 5.** Flexibility of supramolecular glycopolymers influenced bioactivity. (a) The assessment process of osteogenic promotion ability of CT-3F assemblies with different flexibility. CT-3F(S) and CT-3F(L) represented short rods at Day 0 and long fibers at Day 20 formed by CT-3F, respectively. (b) Immunofluorescence staining of the interaction between CT-3F assemblies and cells after incubating for 24 h. Cells were stained for DAPI (nuclei, blue), cell membrane (red) and CT-3F assemblies (green). (c) Quantitively analysis of fluorescence intensity of CT-3F assemblies. (d) RT-qPCR results for OCN mRNA levels in MC3T3-E1 cells treated with CT-3F assemblies. (e) Immunofluorescence staining and corresponding quantitively analysis of OCN proteins after incubating for 10 days. Cells were stained for DAPI (nuclei, blue), OCN protein (green). (f) CD spectra for CT-FFI and CT-4F rods. Plot of mean square end-to-end distance versus internal contour length[28] with resulting persistence lengths (g) and RT-qPCR results for OCN mRNA levels (h) of CT-FFI and CT-4F rods. Data are presented as means ± SD ($n$ = 3, (*) $p < 0.05$, (**) $p < 0.01$, (***) $p < 0.001$, (****) $p < 0.0001$). One-way ANOVA with Tukey posthoc test. (d, e, h).

could not dominate the H-bond formation of CT (Figure S38). To verify this result, HCl and NaOH aqueous solution was added to modulate the contribution from protonation or deprotonation of carboxyl groups in CT-3F (Figure S39) to the assembly behavior, respectively. TEM results showed that CT-3F fibers remained nonhelical after the addition of an acid or base, indicating that electrostatic repulsion did not play a dominant role in this process. Moreover, the potential effect of



https://doi.org/10.1021/jacs.5c18638
J. Am. Chem. Soc. 2026, 148, 8331−8340

electrostatic interactions was also explored in the presence of high concentrations of NaCl (Figure S40). The results showed that the morphology of CT-3F fibers remained unchanged under this condition, further confirming that the weak H-bond forming ability of CT came from its linear geometry rather than increased carboxylic acid groups.

In addition to the H-bond network, glycan geometry may also modulate the mechanical properties of glycopeptide fibers by influencing peptide−glycan−solvent interactions. The simulation results showed that although these two fibers had the similar distribution of SASA, phenylalanine residues in CT-3F fibers exhibited higher SASA values than that in SL-3F ones (see Figures S20 and S29). It was indicated that water was less confined within CT-3F fibers, and CT-3F molecules are more solvated, which was further experimentally supported by the FT-IR spectra (see Figure S41). This increased solvation weakened intermolecular interactions within the fiber, thereby promoting greater fiber flexibility for CT-3F. Together, these results indicated that linear geometry of CT led to less H-bonds and more compliant nonhelical CT-3F fibers, while nonlinear geometry of SL led to stronger H-bond forming and helical SL-3F fibers with different flexibility.

### Mechanical Property of Supramolecular Glycopolymers Influenced Bioactivity

As CS is one of the major ECM constituents for supporting osteoblast performance,[31] we suppose that CT−peptide assemblies could exhibit osteogenic potential, where mechanical properties such as flexibility of glycoassemblies may play an important role. Here, two sets of experiments were designed with different aspects of adjustments. Through controlling the assembly time of CT-3F, both short rods and long fibers could be obtained from the same monomer (Figure 2b), referred to as CT-3F(S) and CT-3F(L), respectively. The length of CT-3F(S) was about 200 nm which was shorter than its persistence length, indicating its much higher rigidity than CT-3F(L). The influence of supramolecular glycopolymer flexibility on their osteogenic capability was investigated through incubating with mouse preosteoblastic MC3T3-E1 cells. The cytotoxicity and stability in culture conditions of these glycopeptide assemblies was examined at first, showing that all assemblies had good biocompatibility and stability (see Figures S42−S46). The interactions of these glycoassemblies with cells were investigated through coassembling with FITC-YFmoc for visualization. After incubation for 24 h, CT-3F(L) exhibited strong interaction with cell surface, while rigid CT-3F(S) showed significantly less interaction with cells (see Figure 5b and 5c, as well as Figure S47). Noncollagenous protein osteocalcin (OCN) was the typical osteoblast differentiation marker to assess osteogenic differentiation.[32,33] Therefore, the OCN mRNA expression level was measured by RT-qPCR to evaluate osteogenic promotion ability of these glycoassemblies after 7-day incubation (Figure 5a). A significant upregulation of OCN expression in cells treated with long fibers was observed (Figure 5d), indicating that long fibers with higher flexibility had much higher bioactivity than rigid short rods. Moreover, the level of expression of the OCN protein was also evaluated and showed a consistent upregulation trend with mRNA data (Figure 5e). We further investigated how the long fibers enhanced osteogenic activity through examining the involvement of CD44, a key cell-surface receptor known to interact with glycoproteins and extracellular matrix components. Our results indicated that the long fibers could bind to CD44 and induce its clustering on the cell surface (Figure S48). These results suggested that the flexibility of glycoassemblies could influence their interaction with cells and the overall bioactivity.

To further verify this, CT-peptide assemblies with different oligopeptide parts were designed to obtain glycoassemblies with different flexibility. Derived from CT-3F, CT-FFI and CT-4F were designed with slightly different oligopeptides (Figure S49). After sonication, CT-FFI and CT-4F both formed short rods with similar lengths according to TEM observation (Figure S50). CD spectra showed that CT-FFI rods had $\beta$-sheet structures, while CT-4F ones were in the $\alpha$-helix conformation (Figure 5f). The flexibility of these two rods was investigated (see Figure 5g, as well as Figure S51). The persistence lengths ($\lambda$) of CT-FFI rods were around 9.7 $\mu$m, and CT-4F rods were about 84 nm. The significantly lower persistence length of CT-4F rods indicated their much higher flexibility than CT-FFI ones, which may be related with their different molecular packing.[34] The characteristics of these two glycoassemblies were further investigated with a combination of TEM, DLS, and SAXS experiments (Figure S52). The results showed that CT-FFI rods remained after further incubation under room temperature, while CT-4F rods grew into long fibers. Therefore, short rods of CT-FFI and CT-4F at Day 0 exhibiting good biocompatibility and stability were incubated with MC3T3 cells to explore their biofunctions (see Figures S42 and S53). After 7 days of incubation, the *Ocn* mRNA expression level of flexible CT-4F rods was significantly improved, while rigid CT-FFI rods showed no promoting effect (Figure 5h). Their interaction with cells was also investigated, and flexible CT-4F rods showed stronger interactions (see Figure S54). Together, glycoassemblies with higher flexibility could lead to a stronger cell interaction and higher osteogenic activity.

## CONCLUSION

In summary, the mechanical properties and biological activity of supramolecular polymers with oligosaccharides were proposed to be investigated both experimentally and theoretically. Glycan geometry was found to play a pivotal role in this process for the first time. Specifically, linear configuration of CT contributed to the relatively weak H-bond forming ability of glycopeptides, resulting in nonhelical fibrils with enhanced structural flexibility. Notably, supramolecular glycopolymers with higher flexibility exhibited stronger cellular interactions and significantly up-regulated osteogenic gene expression. The structural diversity of polysaccharides in PGs and glycoproteins can influence their inherent properties, but the underlying mechanism has remained elusive. This study provided an important experimental example of how glycopeptide fibrous assemblies could be driven by the glycan fragment and elucidated the regulatory role of glycan geometry on mechanical properties of supramolecular fibrils. Our results presented that spatial arrangement of glycans, not merely sulfation pattern or sequence, carried functional instruction and could serve as information encoding for glycobiology. This work is highly relevant both from a fundamental biological perspective trying to understand the role of glycosylation in biological interactions as well as from a material perspective where glycan conjugates offer new opportunities to design and develop biobased and bioinspired materials. In short, our work contributes to a comprehensive understanding of glycans in native fibrous macromolecules and serves as an alternative


https://doi.org/10.1021/jacs.5c18638
J. Am. Chem. Soc. 2026, 148, 8331−8340

strategy for modulating properties of supramolecular polymers and related biomaterials, providing further insights for next-generation biomaterial design.

## ■ ASSOCIATED CONTENT

### Supporting Information

The Supporting Information is available free of charge at https://pubs.acs.org/doi/10.1021/jacs.5c18638.

Experimental materials and characterization; Synthetic procedures; Experimental methods; Characterization of glycopeptide assemblies; Mechanical parameters of glycopeptide fibers; Simulation details and results; details for biological experiments (PDF)

## ■ AUTHOR INFORMATION


### Corresponding Authors

**Long Li** − *The State Key Laboratory of Molecular Engineering of Polymers and Department of Macromolecular Science, Fudan University, Shanghai 200433, China*; Email: long_li@fudan.edu.cn

**Guosong Chen** − *The State Key Laboratory of Molecular Engineering of Polymers and Department of Macromolecular Science, Fudan University, Shanghai 200433, China; Qingdao Research Institute, Fudan University, Shanghai 200433, China*; orcid.org/0000-0001-7089-911X; Email: guosong@fudan.edu.cn

### Authors

**Xiaomei Liu** − *The State Key Laboratory of Molecular Engineering of Polymers and Department of Macromolecular Science, Fudan University, Shanghai 200433, China*

**Liman Zhao** − *Shanghai Key Lab of Chemical Assessment and Sustainability, School of Chemical Science and Engineering, Tongji University, Shanghai 200092, China*

**Pingping Niu** − *Department of Stomatology, Xinhua Hospital, Shanghai Jiao Tong University School of Medicine, Shanghai 200092, China*

**Ya Zeng** − *The State Key Laboratory of Molecular Engineering of Polymers and Department of Macromolecular Science, Fudan University, Shanghai 200433, China*

**Yiwei Shi** − *The State Key Laboratory of Molecular Engineering of Polymers and Department of Macromolecular Science, Fudan University, Shanghai 200433, China*

**Xinyu Bian** − *The State Key Laboratory of Molecular Engineering of Polymers and Department of Macromolecular Science, Fudan University, Shanghai 200433, China*

**Yating Liu** − *The State Key Laboratory of Molecular Engineering of Polymers and Department of Macromolecular Science, Fudan University, Shanghai 200433, China*

**Shengjie Ling** − *The State Key Laboratory of Molecular Engineering of Polymers and Department of Macromolecular Science, Fudan University, Shanghai 200433, China*; orcid.org/0000-0003-1156-0479

Complete contact information is available at: https://pubs.acs.org/10.1021/jacs.5c18638


### Notes

The authors declare no competing financial interest.

## ■ ACKNOWLEDGMENTS

G.C. and L.L. thank NSFC/China (52125303, 52403179, 92356305 and 22431002), the National Key Research and Development Program of China (2023YFA0915300), and Innovation Program of Shanghai Municipal Education Commission (2023ZKZD02) for financial support. S.L. thanks NSFC/China (52322305) for financial support. We thank the Shanghai Synchrotron Radiation Facility (Bio-SAXS: BL19U2) for the SAXS test.

## ■ REFERENCES


(1) He, M.; Zhou, X.; Wang, X. Glycosylation: mechanisms, biological functions and clinical implications. *Sig. Transduct. Target. Ther.* **2024**, *9*, 194.

(2) Brito, A.; Dave, D.; Lampel, A.; Castro, V. I. B.; Kroiss, D.; Reis, R. L.; Tuttle, T.; Ulijn, R. V.; Pires, R. A.; Pashkuleva, I. Expanding the Conformational Landscape of Minimalistic Tripeptides by Their O-Glycosylation. *J. Am. Chem. Soc.* **2021**, *143*, 19703−19710.

(3) Onofrei, D.; Stengel, D.; Jia, D.; Johnson, H. R.; Trescott, S.; Soni, A.; Addison, B.; Muthukumar, M.; Holland, G. P. Investigating the Atomic and Mesoscale Interactions that Facilitate Spider Silk Protein Pre-Assembly. *Biomacromolecules* **2021**, *22*, 3377−3385.

(4) Soares da Costa, D.; Reis, R. L.; Pashkuleva, I. Sulfation of Glycosaminoglycans and Its Implications in Human Health and Disorders. *Annu. Rev. Biomed. Eng.* **2017**, *19*, 1−26.

(5) Hartley, A.; Williams, P. M.; Mata, A. A Comparison of the Mechanical Properties of ECM Components and Synthetic Self-Assembling Peptides. *Adv. Healthc. Mater.* **2025**, *14*, 2402385.

(6) Clausen, T. M.; Sandoval, D. R.; Spliid, C. B.; Pihl, J.; Perrett, H. R.; Painter, C. D.; Narayanan, A.; Majowicz, S. A.; Kwong, E. M.; McVicar, R. N.; Thacker, B. E.; Glass, C. A.; Yang, Z.; Torres, J. L.; Golden, G. J.; Bartels, P. L.; Porell, R. N.; Garretson, A. F.; Laubach, L.; Feldman, J.; Yin, X.; Pu, Y.; Hauser, B. M.; Caradonna, T. M.; Kellman, B. P.; Martino, C.; Gordts, P. L. S. M.; Chanda, S. K.; Schmidt, A. G.; Godula, K.; Leibel, S. L.; Jose, J.; Corbett, K. D.; Ward, A. B.; Carlin, A. F.; Esko, J. D. SARS-CoV-2 Infection Depends on Cellular Heparan Sulfate and ACE2. *Cell* **2020**, *183*, 1043−1057.

(7) Chaudhuri, O.; Cooper-White, J.; Janmey, P. A.; Mooney, D. J.; Shenoy, V. B. Effects of extracellular matrix viscoelasticity on cellular behaviour. *Nature* **2020**, *584*, 535−546.

(8) Karamanos, N. K.; Piperigkou, Z.; Theocharis, A. D.; Watanabe, H.; Franchi, M.; Baud, S.; Brézillon, S.; Götte, M.; Passi, A.; Vigetti, D.; Ricard-Blum, S.; Sanderson, R. D.; Neill, T.; Iozzo, R. V. Proteoglycan Chemical Diversity Drives Multifunctional Cell Regulation and Therapeutics. *Chem. Rev.* **2018**, *118*, 9152−9232.

(9) Kramer, J. R.; Onoa, B.; Bustamante, C.; Bertozzi, C. R. Chemically tunable mucin chimeras assembled on living cells. *Proc. Natl. Acad. Sci. U.S.A.* **2015**, *112*, 12574−12579.

(10) Goor, O. J. G. M.; Hendrikse, S. I. S.; Dankers, P. Y. W.; Meijer, E. W. From supramolecular polymers to multi-component biomaterials. *Chem. Soc. Rev.* **2017**, *46*, 6621−6637.

(11) Rijns, L.; Rutten, M. G. T. A.; Vrehen, A. F.; Aldana, A. A.; Baker, M. B.; Dankers, P. Y. W. Mimicking the extracellular world: from natural to fully synthetic matrices utilizing supramolecular biomaterials. *Nanoscale* **2024**, *16*, 16290−16312.

(12) Lee, S. S.; Fyrner, T.; Chen, F.; Álvarez, Z.; Sleep, E.; Chun, D. S.; Weiner, J. A.; Cook, R. W.; Freshman, R. D.; Schallmo, M. S.; Katchko, K. M.; Schneider, A. D.; Smith, J. T.; Yun, C.; Singh, G.; Hashmi, S. Z.; McClendon, M. T.; Yu, Z.; Stock, S. R.; Hsu, W. K.; Hsu, E. L.; Stupp, S. I. Sulfated glycopeptide nanostructures for multipotent protein activation. *Nat. Nanotechnol.* **2017**, *12*, 821−829.

(13) Su, L.; Hendrikse, S. I. S.; Meijer, E. W. Supramolecular glycopolymers: How carbohydrates matter in structure, dynamics, and function. *Curr. Opin. Chem. Biol.* **2022**, *69*, 102171.

(14) Hendrikse, S. I. S.; Su, L.; Hogervorst, T. P.; Lafleur, R. P. M.; Lou, X.; van der Marel, G. A.; Codee, J. D. C.; Meijer, E. W. Elucidating the Ordering in Self-Assembled Glycocalyx Mimicking

Supramolecular Copolymers in Water. *J. Am. Chem. Soc.* **2019**, *141*, 13877−13886.
(15) Yang, J.; Du, Q.; Li, L.; Wang, T.; Feng, Y.; Nieh, M.-P.; Sheng, J.; Chen, G. Glycosyltransferase-Induced Morphology Transition of Glycopeptide Self-Assemblies with Proteoglycan Residues. *ACS Macro Lett.* **2020**, *9*, 929−936.
(16) Helmers, I.; Ghosh, G.; Albuquerque, R. Q.; Fernández, G. Pathway and Length Control of Supramolecular Polymers in Aqueous Media via a Hydrogen Bonding Lock. *Angew. Chem., Int. Ed.* **2021**, *60*, 4368−4376.
(17) Zhang, Z.; Xue, C.-C.; Feng, Y.-L.; Chen, G.-S. Chemical Synthesis of Globo H and Mannobiose Glycopolymers and their Immunological Stimulation. *Chin. J. Polym. Sci.* **2024**, *42*, 1661−1667.
(18) Bellan, R.; Rutten, M. G. T. A.; Lou, X.; Wallace, C. M.; Rovers, M. M.; Smith, A. J.; van Genderen, M. H. P.; Adams, D. J.; Dankers, P. Y. W. Tuning the Supramolecular Polymerization and Cell Response of Ureidopyrimidinone Monomers by Pushing the Hydrophobic Threshold. *J. Am. Chem. Soc.* **2025**, *147*, 21478−21491.
(19) Yuan, S. C.; Álvarez, Z.; Lee, S. R.; Pavlović, R. Z.; Yuan, C.; Singer, E.; Weigand, S. J.; Palmer, L. C.; Stupp, S. I. Supramolecular Motion Enables Chondrogenic Bioactivity of a Cyclic Peptide Mimetic of Transforming Growth Factor-$\beta$1. *J. Am. Chem. Soc.* **2024**, *146*, 21555−21567.
(20) Kim, T.; Hong, J.; Kim, J.; Cho, J.; Kim, Y. Two-Dimensional Peptide Assembly via Arene−Perfluoroarene Interactions for Proliferation and Differentiation of Myoblasts. *J. Am. Chem. Soc.* **2023**, *145*, 1793−1802.
(21) Rajesh, A.; Sajeev, D.; R, N. K.; Rangasamy, J.; Nair, S. C. Chondroitin sulfate: From bioactive molecule to versatile drug delivery system for advancing regenerative medicine. *Int. J. Biol. Macromol.* **2025**, *311*, 143746.
(22) Pérez-Madrigal, M. M.; Gil, A. M.; Casanovas, J.; Jiménez, A. I.; Macor, L. P.; Alemán, C. Self-assembly pathways in a triphenylalanine peptide capped with aromatic groups. *Colloid Surface. B* **2022**, *216*, 112522.
(23) Shivhare, V.; Gupta, A.; Ahuja, R.; Barde, D.; Ahirwar, S. K.; Basu, A.; Konar, A. D. A novel 16-hydroxy-palmitic acid tethered d-configured homo-chiral triphenylalanine based nanofibrillar scaffold with innate anticancer potential. *Chem. Commun.* **2025**, *61*, 9717−9720.
(24) Gilboa, B.; Lafargue, C.; Handelman, A.; Shimon, L. J. W.; Rosenman, G.; Zyss, J.; Ellenbogen, T. Strong Electro-Optic Effect and Spontaneous Domain Formation in Self-Assembled Peptide Structures. *Adv. Sci.* **2017**, *4*, 1700052.
(25) Feng, Y.; Li, L.; Du, Q.; Gou, L.; Zhang, L.; Chai, Y.; Zhang, R.; Shi, T.; Chen, G. Polymorphism of Kdo-Based Glycolipids: The Elaborately Determined Stable and Dynamic Bicelles. *CCS Chem.* **2022**, *4*, 2228−2238.
(26) Liu, R.; Zhang, R.; Li, L.; Kochovski, Z.; Yao, L.; Nieh, M.-P.; Lu, Y.; Shi, T.; Chen, G. A Comprehensive Landscape for Fibril Association Behaviors Encoded Synergistically by Saccharides and Peptides. *J. Am. Chem. Soc.* **2021**, *143*, 6622−6633.
(27) Adamcik, J.; Jung, J.-M.; Flakowski, J.; De Los Rios, P.; Dietler, G.; Mezzenga, R. Understanding amyloid aggregation by statistical analysis of atomic force microscopy images. *Nat. Nanotechnol.* **2010**, *5*, 423−428.
(28) Usov, I.; Mezzenga, R. FiberApp: An Open-Source Software for Tracking and Analyzing Polymers, Filaments, Biomacromolecules, and Fibrous Objects. *Macromolecules* **2015**, *48*, 1269−1280.
(29) Yang, S.; Zhao, C.; Yang, Y.; Ren, J.; Ling, S. The Fractal Network Structure of Silk Fibroin Molecules and Its Effect on Spinning of Silkworm Silk. *ACS Nano* **2023**, *17*, 7662−7673.
(30) Knowles, T. P.; Fitzpatrick, A. W.; Meehan, S.; Mott, H. R.; Vendruscolo, M.; Dobson, C. M.; Welland, M. E. Role of Intermolecular Forces in Defining Material Properties of Protein Nanofibrils. *Science* **2007**, *318*, 1900−1903.
(31) Paganini, C.; Costantini, R.; Superti-Furga, A.; Rossi, A. Bone and connective tissue disorders caused by defects in glycosaminoglycan biosynthesis: a panoramic view. *FEBS J.* **2019**, *286*, 3008−3032.
(32) He, B.; Zhang, M.; Yin, L.; Quan, Z.; Ou, Y.; Huang, W. bFGF-incorporated composite biomaterial for bone regeneration. *Mater. Des.* **2022**, *215*, 110469.
(33) Rasool, N.; Negi, D.; Singh, Y. Thiol-Functionalized, Antioxidant, and Osteogenic Mesoporous Silica Nanoparticles for Osteoporosis. *ACS Biomater. Sci. Eng.* **2023**, *9*, 3535−3545.
(34) VandenAkker, C. C.; Engel, M. F. M.; Velikov, K. P.; Bonn, M.; Koenderink, G. H. Morphology and Persistence Length of Amyloid Fibrils Are Correlated to Peptide Molecular Structure. *J. Am. Chem. Soc.* **2011**, *133*, 18030−18033.




https://doi.org/10.1021/jacs.5c18638
J. Am. Chem. Soc. 2026, 148, 8331−8340